http://www.jstage.jst.go.jp/browse/biophysics

BIOPHYSICS

Vol. 4, pp. 19–28 (2008)
doi: 10.2142/biophysics.4.19

Correlation between square of electron tunneling matrix element and donor-acceptor distance in fluctuating protein media

Hirotaka Nishioka[1], Nobuharu Ueda[2] and Toshiaki Kakitani[1,2]

[1]*Graduate School of Environmental and Human Sciences, Meijo University, Tempaku-ku, Nagoya 468-8502, Japan*
[2]*Department of General Education, Faculty of Science and Technology, Meijo University, Tempaku-ku, Nagoya 468-8502, Japan*

Received 2 July, 2008; accepted 17 September, 2008

Correlation between fluctuations of the square of electron tunneling matrix element T_{DA}^2 and the donor-acceptor distance R_{DA} in the electron transfer (ET) reaction from bacteriopheophytin anion to the primary quinone of the reaction center in the photosynthetic bacteria *Rhodobacter sphaeroides* is investigated by a combined study of molecular dynamics simulations of the protein conformation fluctuation and quantum chemical calculations. We adopted two kinds of R_{DA}; edge-to-edge distance R_{EE} and center-to-center distance R_{CC}. The value of T_{DA}^2 distributed over more than 5 orders of magnitude and the fluctuation of the value of R_{DA} distributed over more than 1.8 Å for the 10^6 instantaneous conformations of 1 ns simulation. We made analysis of the time-averaged correlation step by step as follows. We divide the 10^6 simulation data into 1000/t parts of small data set to obtain the averaged data points of $\langle T_{DA}^2\rangle_t$ and $\langle R_{EE}\rangle_t$ or $\langle R_{CC}\rangle_t$. Plotting the 1000/t sets of $\log_{10}\langle T_{DA}^2\rangle_t$ as a function of $\langle R_{EE}\rangle_t$ or $\langle R_{CC}\rangle_t$, we made a principal coordinate analysis for these distributions. The slopes $\langle\beta_E\rangle_t$ and $\langle\beta_C\rangle_t$ of the primary axis are very large at small value of t and they are decreased considerably as t becomes large. The ellipticity for the distribution of $\langle T_{DA}^2\rangle_t$ *vs* $\langle R_{EE}\rangle_t$ which can be a measure for the degree of correlation became very small when t is large, while it does not hold for the distribution of $\langle T_{DA}^2\rangle_t$ *vs* $\langle R_{CC}\rangle_t$. These results indicate that only the correlation between $\langle T_{DA}^2\rangle_t$ and $\langle R_{EE}\rangle_t$ for large t satisfies the well-known linear relation ("Dutton law"), although the slope is larger than the original value 1.4 Å^{-1}. Based on the present result, we examined the analysis of the dynamic disorder by means of the single-molecule spectroscopy by Xie and co-workers with use of the "Dutton law".

Key words: protein fluctuation, donor-acceptor distance, electron transfer rate, Dutton law, photosynthetic reaction center

Corresponding author: Hirotaka Nishioka, Graduate School of Environmental and Human Sciences, Meijo University, Tempaku-ku, Nagoya 468-8502, Japan. e-mail: nishioka@ccmfs.meijo-u.ac.jp

The electron transfer (ET) in biological systems takes place by means of the electron tunneling between donor (D) and acceptor (A) in protein media. Usually the distance between the donor and acceptor in such ET is separated by 5–20 Å. In order to make such a long-range ET possible, the superexchange mechanism in which the electronic state of the protein media is virtually incorporated into the electronic states of donor and acceptor to facilitate the electron tunneling works[1]. The electron tunneling proceeds by passing the bonds with lower energy barriers and the spaces with shorter distance under the restriction that the overall pathway length should be short as much as possible[2]. As a result, the chosen tunneling pathways and the ET rate are expected to be sensitive to the kind of protein conformation[3].

Experimentally it was found that the ET rate k_{DA} in protein media has much correlation with the donor-acceptor distance R_{DA} as follows:

$$k_{DA} = 10^{13}\exp(-\beta(R_{DA}-3.6))\ (\mathrm{s}^{-1}), \qquad (1)$$

where β is a parameter with a value 1.4 Å^{-1} [4]. Here, the distance was obtained by calculating the edge-to-edge distance of π-orbitals of donor and acceptor molecules with the

closest distance. This relation was obtained by combining the various data of photosynthetic ET systems and others in stationary state. We call this empirical relation the "Dutton law" hereafter. More sophisticated form of the "Dutton law" was also given with a concept of the packing density of atoms[5].

Theoretically, the ET rate k_{DA} in the elastic tunneling mechanism[6] is written as follows[1]:

$$k_{DA}=\frac{2\pi}{\hbar}<T_{DA}^2>(FC), \qquad (2)$$

where < > represents the thermal average and (FC) denote the thermally averaged Franck-Condon factor or called the nuclear factor. Marcus showed that (FC) is expressed by the Gaussian function of the free energy difference ΔG between the initial and final states, which is called the Marcus energy gap law[1].

The R_{DA}-dependence of (FC) enters through the reorganization energy and the energy gap. However, those R_{DA}-dependences are weak so far as the R_{DA} is larger than about 5 Å[7,8], which applies to many redox proteins. The R_{DA}-dependence in equation (1) mostly comes from the R_{DA}-dependence of $<T_{DA}^2>$. Therefore, we write

$$<T_{DA}^2>=A\exp(-\beta<R_{DA}>), \qquad (3)$$

where A is a constant and we replaced R_{DA} with the average value $<R_{DA}>$ because the x-ray crystallographic value of R_{DA} is already averaged. Equation (3) is the relation obtained in the ordinary thermal equilibrium state.

On the other hand, recent theoretical calculations using the MD simulations and quantum chemistry showed that instantaneous values of the electron tunneling matrix element T_{DA} are greatly varied under the fluctuation of the protein conformation[9]. The protein conformational fluctuation involves the fluctuation of conformation of amino acids as well as the fluctuation of donor-acceptor distance R_{DA}. Recently experimental studies using the single-molecule spectroscopy were made for extracting dynamical information of the function and the mechanism of proteins[10–13]. In such case, protein conformation fluctuation plays a significant role. In some case, the conformation fluctuation with time scale longer than the biochemical reaction is present. This slow fluctuation was called the dynamic disorder[14]. Under such situation, Xie and co-workers exploited a new experimental technique to derive this dynamic disorder using the fluorescence quenching phenomenon due to the ET reaction[15,16]. When the distance between the fluorescer and the quencher is small, the ET reaction rate is large and the fluorescence quenching time is reduced and *vice versa*. By observing the fluctuation of the fluorescence quenching time, the fluctuation of the ET rate was obtained, and the fluctuation of the fluorescer-quencher distance was calculated by using the "Dutton law" of equation (1). Applying this new method of single-molecule spectroscopy combined with the photon-by-photon technique[15,16] to flavin reductase, Xie and co-workers obtained a detailed information of the dynamic disorder of protein in the time range of milliseconds to minutes[17,18]. From this result, they derived power law of the distance autocorrelation function. These results together with their earlier study[13] prompted many theoretical studies[19–23].

Here, there remains a question whether the similar relation to the "Dutton law" holds between the fluctuating ET rate and the fluctuating distance R_{DA} in single protein. So far, no one examined this problem in protein environment, although some calculations were made for the fluctuating ET in solutions[24,25].

In the present study, we theoretically examine what kind of relationship holds between the fluctuating ET rate and fluctuating R_{DA}. Based on this analysis, we examine the validity of using the "Dutton law" in the analysis of the dynamic disorder. The constitution of this paper is as follows: In the Method section, the calculation method is described. We applied the method to the ET from the bacteriopheophytin anion ($BPhe^-$) to the primary quinone (Q_A) in the bacterial photosynthetic reaction center (BPRC) of *Rhodobacter sphaeroides*. In the Results section the results are presented. The Discussion section is devoted to the discussion. In the Conclusion section conclusion is made.

Method

The procedures for the MD simulations are the same as before[6,9,33]. Here, we briefly describe it. The initial configuration of the reaction center (RC) was obtained from the Protein Data Bank, entry code 1AIJ [26]. The MD simulations are performed for the whole RC including 828 amino acids, all cofactors, 262 water molecules, and 4 detergent molecules of lauryldimethylamineoxide (LDAO) which are attached on the surface of the RC. The phytil chain of the primary quinine is included up to C31. We restrict the position of the hydrophobic phytil chain in the region C21 to C31 since the carbon atoms of this region are located outside the protein surface and no LDAO molecule is attached to them[33]. The MD program PRESTO[27] was used with the AMBER force field[28]. The SHAKE algorithm[29] was used for bond stretchings of hydrogen atoms. We first obtained the energy minimum conformation of protein. Then, the temperature T of the system was gradually elevated to 300 K. Integration time step of 1 fs was employed. After 600 ps run for equilibration, we generated a trajectory for 1 ns. We collected the conformations of 10^6 at every 1 fs, which were used to calculate T_{DA} and R_{DA}.

The procedures for the quantum chemistry (QC) calculations of T_{DA} are the same as before[6,9]. Here, we briefly describe it. The chemical structures of donor and acceptor which we adopted in calculating the molecular orbitals of donor and acceptor are shown in Figure 1. In these calculations, long hydrocarbon chains of native bacteriopheophytin *a* and the native ubiquinone 10 are truncated to hydrogen

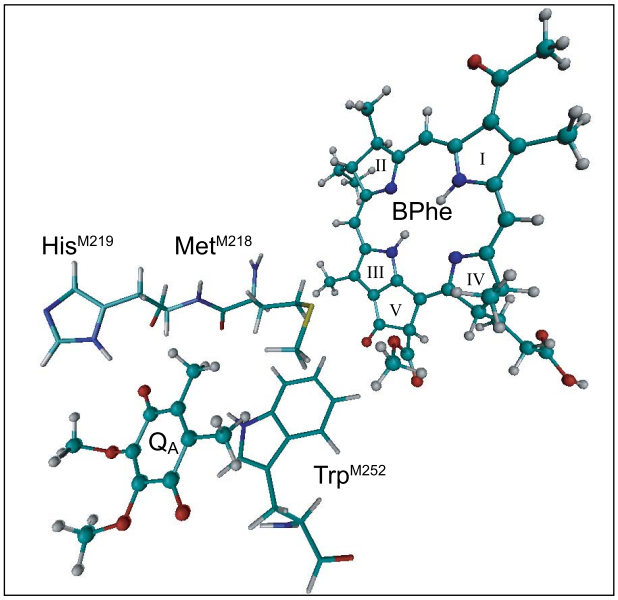

Figure 1 General view of the coordination of donor (bacteriopheophytin), acceptor (quinone), and the three amino acids (Trp^{M252}, Met^{M218}, and His^{M219}) which we investigate in this paper. The molecular structure of donor and acceptor is represented by a ball and stick model. The molecular structure of the three amino acids is represented by a stick model. Blue balls, red balls, deep blue balls, and white balls indicate carbon atoms, oxygen atoms, nitrogen atoms, and hydrogen atoms, respectively. The gold stick in the Met^{M218} represents the sulfur atom.

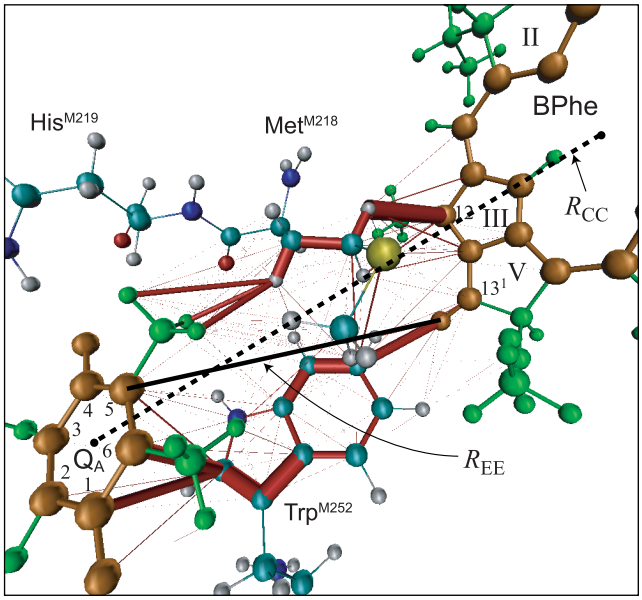

Figure 2 Visualization of the edge-to-edge distance (black straight line) and the center-to-center distance (black broken line) drawn on the calculated map of the mean-square tunneling currents corrected by the quantum-interference $<\tilde{J}_{ab}^{2}>$ (taken from Ref. 33). Protein conformation together with that of donor and acceptor are drawn by the ball and stick model. The orange and green balls indicate the atoms constituting the conjugated part and non-conjugated part of donor and acceptor, respectively. The red pipes represent the electron tunneling pathways whose widths are proportional to the magnitude of $<\tilde{J}_{ab}^{2}>$. We observed two main tunneling routes: Trp route passing through Trp residue and Met route passing through a part of Met.

atoms. It has been shown that the similar result of the time variation of T_{DA} is obtained in both cases when 60 amino acids surrounding donor and acceptor are considered and when 3 amino acids between donor and acceptor are considered[9]. Then we consider the three amino acids Trp^{M252}, Met^{M218}, and His^{M219} in the present calculations. The coordination of the three amino acids is shown in Figure 1. The electronic structure of donor and acceptor were calculated by the PM3 method[30] in the Gaussian package[31]. To save the computation time, we fix the atomic orbital coefficients in the molecular orbitals which are solved in the isolated state of BPhe and Q_A. The electronic structures of the pruned protein are solved at the extended Hückel level. We referred to the FORTICON8 program[32]. We take into account the variable hyperconjugation effect of the methyl group with the π-conjugated part of quinone in the course of rotation of the methyl group[33]. The tunneling matrix element T_{DA} is calculated for each protein conformation by the same method as before[6,9]. The tunneling energy is chosen at −9.5 eV.

Results

We first define two kinds of the distance between donor and acceptor. The first is the shortest edge-to-edge distance of π-conjugated region, R_{EE}, which measures between oxygen atom bonded to $C13^1$ of BPhe and C6 of Q_A. This kind of edge-to-edge distance was used by the Dutton group[4]. The second is the center-to-center distance R_{CC} which measures the distance between the center of the polycyclic ring of BPhe and the center of the aromatic ring of Q_A. This kind of distance was used by Luo *et al.*[23]. In Figure 2 we represents these two kinds of distance by the straight line (R_{EE}) and the dotted line (R_{CC}). In the same Figure, the average tunneling routes (Trp route and Met route) which were recently obtained are drawn by the red pipes (the pipe width is proportional to the magnitude of the mean-square of the tunneling current corrected by the quantum interference effect)[33]. The distance R_{EE} is closely along the Trp route and roughly along the Met route.

In Figure 3 we show a typical example of the time variation of T_{DA}^{2}. We find that T_{DA}^{2} changes very quickly (in tens fs) and the very sharp peaks appear randomly. Such quick fluctuations of T_{DA}^{2} also occurs in the other redox proteins[34–37].

In Figure 4 we show the calculated correlation diagram of $\log T_{DA}^{2}$ and R_{EE}. In this diagram, the 10,000 data points were plotted at every 100 fs from the simulation data of 1 ns. We find that the values of T_{DA}^{2} distribute over more than 5 orders of magnitude for the distribution of about 2 Å of R_{EE}. We see that very little correlation exists between the values of $\log T_{DA}^{2}$ and R_{EE} calculated for the instantaneous conformations of fluctuating protein.

In Figure 5 we plotted the correlation diagram of $\log T_{DA}^{2}$

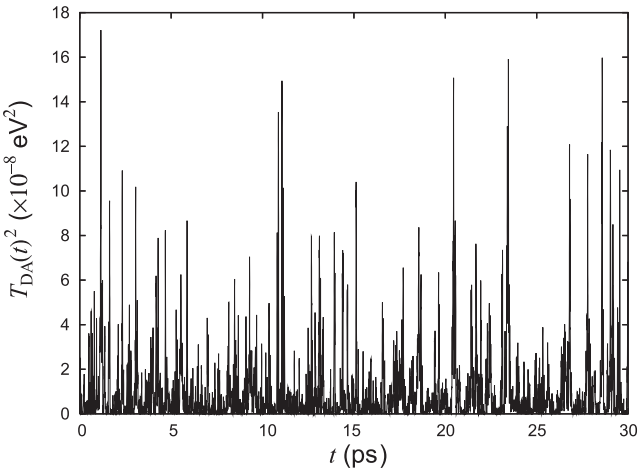

Figure 3 Example of rapid variations of T_{DA}^2 as a function of time t.

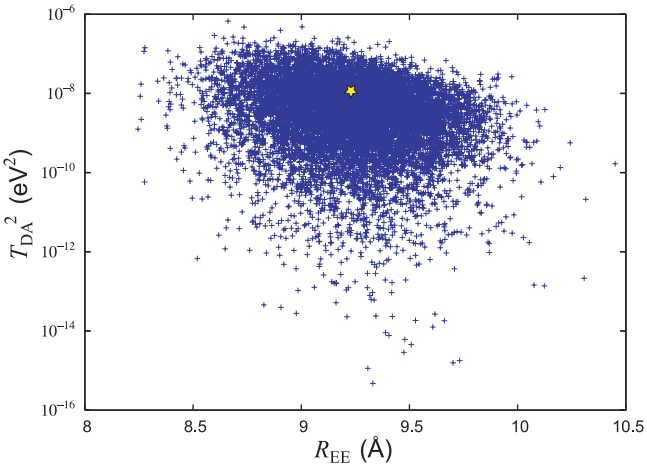

Figure 4 Plot of T_{DA}^2 as a function of R_{EE} for the 10^4 points at every 100 fs in the 1 ns simulation data. The averaged point is shown by the yellow star.

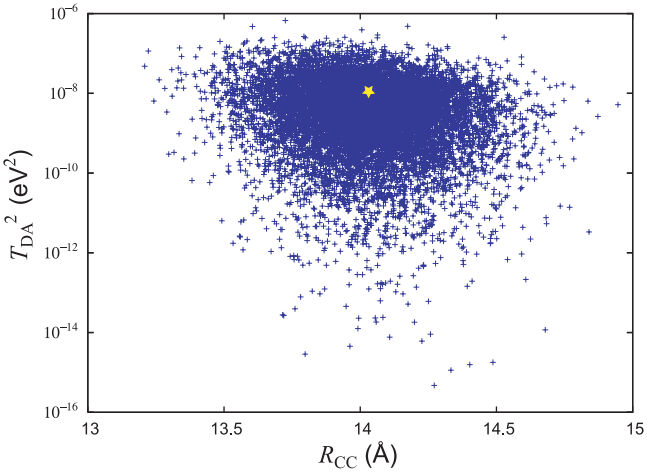

Figure 5 Plot of T_{DA}^2 as a function of R_{CC} for the 10^4 points at every 100 fs in the 1 ns simulation data. The averaged point is shown by the yellow star.

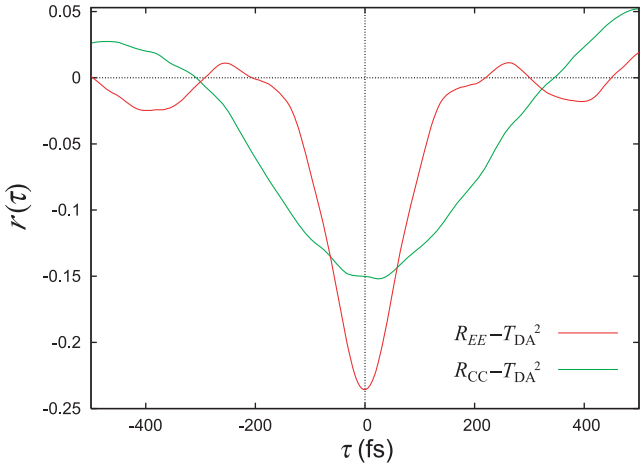

Figure 6 Plot of the mutual correlation function $r(\tau)$ for T_{DA}^2 and R_{EE} or R_{CC}.

and R_{CC} calculated by same way as Figure 4. We find that the values of T_{DA}^2 distribute over more than 5 orders of magnitude for the distribution of about 1.8 Å of R_{CC}. In this case also we find very little correlation between the values of log T_{DA}^2 and R_{CC} calculated for the instantaneous conformations of fluctuating protein.

Next, we investigate the dynamical property of the correlation between T_{DA}^2 and R_{EE} or R_{CC}. We calculate the mutual correlation function $r(\tau)$ as follows

$$r(\tau)=\frac{<(T_{DA}^2(t)-<T_{DA}^2>_T)\,(R_{DA}(t+\tau)-<R_{DA}>_T)>_T}{\sqrt{<(T_{DA}^2(t)-<T_{DA}^2>_T)^2>_T\cdot<(R_{DA}(t)-<R_{DA}>_T)^2>_T}} \tag{4}$$

where $<>_T$ denotes the average taken for the time range T, R_{DA} is R_{EE} or R_{CC}, and τ is the delay time between T_{DA}^2 and R_{DA}.

We calculated $r(\tau)$ using the 10^6 sets of data for T_{DA}^2 and R_{DA} in the time range $T=1$ ns. In Figure 6, we plotted the calculated $r(\tau)$ as a function of τ by the red curve in case of $R_{DA}=R_{EE}$ and the green curve in case of $R_{DA}=R_{CC}$. We find that $r(\tau)$ of the red curve has a rather sharp peak while $r(\tau)$ of the green curve has broad peak. We also find that these $r(\tau)$'s are almost symmetrical with respect to $\tau=0$. The value of $r(0)$ in the case $R_{DA}=R_{EE}$ or $R_{DA}=R_{CC}$ is −0.23 or −0.15, respectively. The value of $|r(0)|$ represents how much synchronously the variation of T_{DA}^2 takes place with that of R_{DA}. The maximum value of $|r(0)|$ is 1. The sign of $r(0)$ is plus or minus depending on the variation of T_{DA}^2 is in phase or out of phase with that of R_{DA}. The above value of $r(0)$ for R_{DA} denotes that the variations of T_{DA}^2 and R_{DA} are out of phase with a certain amount of synchronism to one another. The smaller value of $|r(0)|$ for R_{CC} denotes that the degree of synchronism is smaller than that for R_{EE}. We define the time where the value of $r(\tau)$ becomes $1/e$ time of $r(0)$ as the mutual correlation time τ_c. We read 90 fs for the red curve

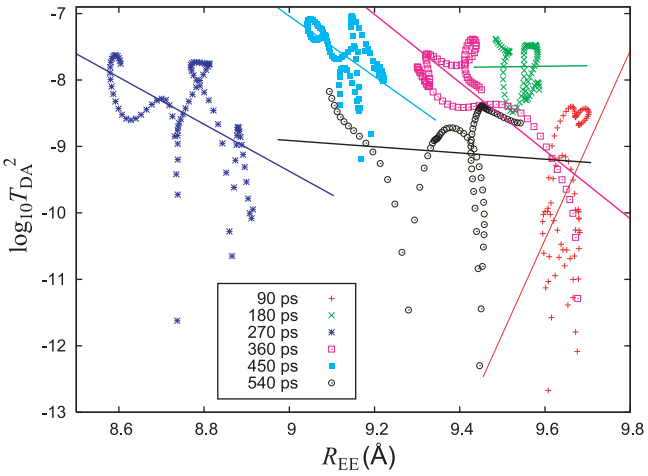

Figure 7 Traces of the data points of $\log_{10} T_{DA}^2$ *vs* R_{EE} for 90 fs starting from the time at 90, 180, 270, 360, 450, and 540 ps in the 1 ns simulation data. The straight line is the best fitted line to equation (5).

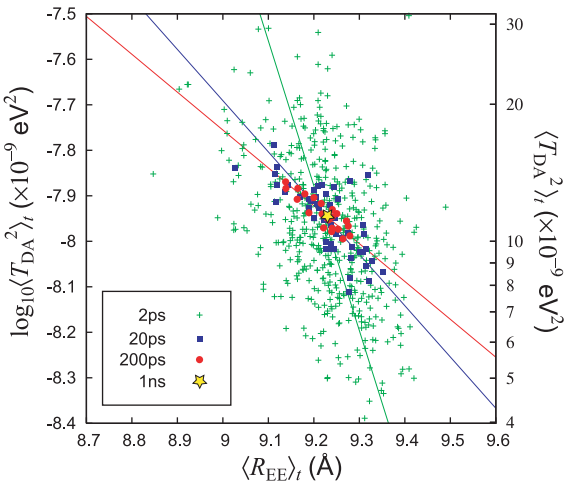

Figure 8 Plot of $\log_{10}\langle T_{DA}^2\rangle_t$ as a function of $\langle R_{EE}\rangle_t$ for three kinds of t (2, 20, and 200 ps). The primary axis for the distribution of each time average is drawn. The totally averaged point is represented by the yellow star.

and 240 fs for the green curve in Figure 6. We consider that the dynamical correlation between the fluctuations of T_{DA}^2 and R_{DA} continues on time scale of τ_c. Therefore, we can say that the dynamical correlation between T_{DA}^2 and R_{CC} is maintained for larger time than that between T_{DA}^2 and R_{EE}. In Figure 7, we plotted the traces of the data points of $\log_{10} T_{DA}^2$ and R_{EE} during the time τ_c starting from six typical times in the 1 ns simulation. We see that the traces of the data points abruptly change. We tried to fit the data points to the following linear function

$$\ln T_{DA}^2 = \alpha_E - \beta_E R_{EE} \qquad (5)$$

The straight lines in Figure 7 show those fitted lines. We observe that the slope β_E changes abruptly form traces to traces. This fact indicates that almost no dynamical correlation exists between $\ln T_{DA}^2$ and R_{EE} in the very short time range of tens fs. The similar result was obtained for $\ln T_{DA}^2$ and R_{CC}.

Next we investigate the correlation between T_{DA}^2 and R_{DA} by taking time average step by step. We divide the 1 ns simulation data (10^6 data points) into $1000/t$ parts of time length t to obtain the averages $\langle T_{DA}^2\rangle_t$ and $\langle R_{EE}\rangle_t$ or $\langle R_{CC}\rangle_t$. When t is very large, the number of the averaged data points of $\langle T_{DA}^2\rangle_t$, $\langle R_{EE}\rangle_t$ and $\langle R_{CC}\rangle_t$ is very small. In such case, we shift the starting time for dividing the 1 ns simulation data in plural ways until we can obtain more than 20 averaged data points. For example, when t=200 ps, we adopt the starting times for dividing the simulation data at $40i$ ps (i=0, ..., 3) to give 21 averaged data points as a total. In Figure 8, we showed the calculated diagram between $\log_{10}\langle T_{DA}^2\rangle_t$ and $\langle R_{EE}\rangle_t$ for three kinds of t; 2, 20, and 200 ps represented by the symbols of green plus, blue closed square and red closed circles, respectively. We also marked the totally averaged (for 1 ns) values of $\log_{10}\langle T_{DA}^2\rangle_t$ and $\langle R_{EE}\rangle_t$ by the yellow star. We see that the distribution of the averaged data points appears to converge to a straight line as t becomes large. Then, we try to fit the averaged data points to the following function:

$$\ln\langle T_{DA}^2\rangle_t = \langle\alpha_E\rangle_t - \langle\beta_E\rangle_t \langle R_{EE}\rangle_t \qquad (6)$$

For this purpose, we made the principal coordinate analysis for the scattered data points. Here, we treat the coordinate $\log_{10}\langle T_{DA}^2\rangle_t$ and the coordinate $\langle R_{EE}\rangle_t$ equivalently in the analysis. The primary axis corresponds to the linear function of equation (6). Then, we calculated the standard deviation $\langle\sigma_1\rangle_t$ along the primary axis, the standard deviation $\langle\sigma_2\rangle_t$ along the secondary axis, and the ratio $\langle\sigma_2\rangle_t/\langle\sigma_1\rangle_t$ ($\equiv\langle\varepsilon\rangle_t$) which is the ellipticity when the distribution of the averaged data points for each t is approximated as ellipsoid as a whole. In Table 1 we listed the calculated values of the slope $\langle\beta_E\rangle_t$ and the ellipticity $\langle\varepsilon\rangle_t$ for 8 kinds of t. We see that $\langle\beta_E\rangle_t$ is very large at small value of t and it is decreased smoothly as t is increased ($\langle\beta_E\rangle_t$=8.452 for t=1 ps; $\langle\beta_E\rangle_t$=1.817 for t=333 ps). We have drawn these primary axes for t=2, 20, and 200 ps by the green, blue, and red lines, respectively, in Figure 8. We clearly observe that the slope of the primary axis decreases very much with time. In Table 1, we see that $\langle\varepsilon\rangle_t$ remains at a constant level of

Table 1 Calculated values of the slope $\langle\beta_E\rangle_t$ and ellipticity $\langle\varepsilon\rangle_t$ for some typical average times in the case of edge-to-edge distance

t	$\langle\beta_E\rangle_t$ (Å^{-1})	$\langle\varepsilon\rangle_t$
1 ps	8.452	0.486
2 ps	7.327	0.484
5 ps	4.206	0.519
10 ps	3.085	0.481
20 ps	2.594	0.399
100 ps	2.166	0.262
200 ps	1.916	0.251
333 ps	1.817	0.155

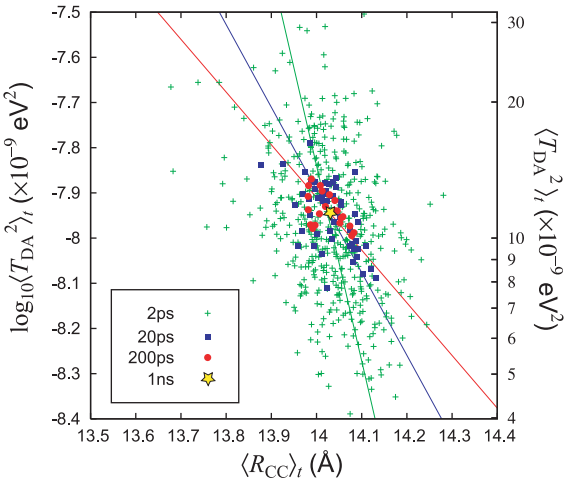

Figure 9 Plot of $\log_{10}\langle T_{DA}^2\rangle_t$ as a function of $\langle R_{CC}\rangle_t$ for three kinds of t (2, 20, and 200 ps). The primary axis for the distribution of each time average is drawn. The totally averaged point is represented by the yellow star.

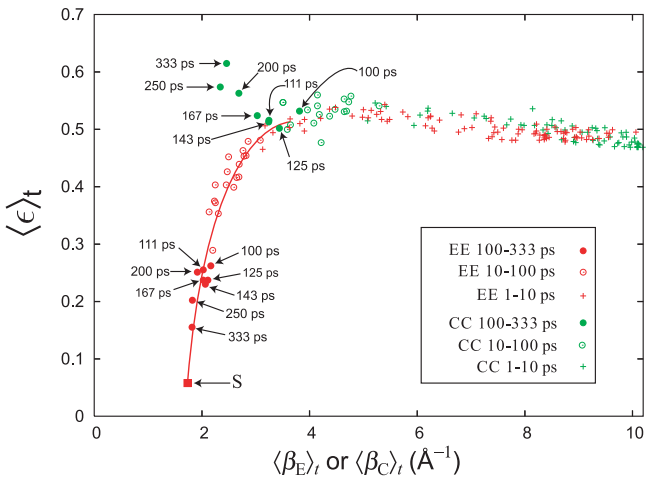

Figure 10 Plot of $\langle\varepsilon\rangle_t$ *vs* $\langle\beta_E\rangle_t$ or $\langle\beta_C\rangle_t$ for the various values of t. The red pluses represent the data points for the time in the range 1–10 ps, the red open circles represent the data points for the time in the range 10–100 ps and the red closed circles represent the data points for the time in the range 100–333 ps for the edge-to-edge distance. The red solid line is extrapolation to the larger time. The red square denoted by S represents the data point of $\langle\varepsilon\rangle_S$ and $\langle\beta_E\rangle_S$ in the stationary state. The green symbols are the data points for the center-to-center distance. The notation is the same as that of the red symbols.

about 0.5 until about 10 ps and then it rapidly decreases down to 0.155 as t is increased from 10 ps to 333 ps. When the ellipticity is small, we can say that the correlation between $\log_{10}\langle T_{DA}^2\rangle_t$ and $\langle R_{EE}\rangle_t$ is very strong. Then, we conclude that the correlation between $\log_{10}\langle T_{DA}^2\rangle_t$ and $\langle R_{EE}\rangle_t$ becomes stronger and converges to a straight line more and more as t is increased.

We also calculated the correlation diagram of $\log_{10}\langle T_{DA}^2\rangle_t$ and $\langle R_{CC}\rangle_t$ and plotted in Figure 9. We fit the data points to the following linear function:

$$\ln\langle T_{DA}^2\rangle_t = \langle\alpha_C\rangle_t - \langle\beta_C\rangle_t\langle R_{CC}\rangle_t \qquad (7)$$

Then, we made the principal coordinate analysis for the scattered data points for each time. In Table 2 we listed the calculated values of the slope $\langle\beta_C\rangle_t$ and the ellipticity $\langle\varepsilon\rangle_t$ for 8 kinds of t. We see that $\langle\beta_C\rangle_t$ is large at small value of t and it is decreased as t is increased ($\langle\beta_C\rangle_t$=8.944 for t=1 ps; $\langle\beta_C\rangle_t$=2.456 for t=333 ps). We also see that $\langle\varepsilon\rangle_t$ remains almost at the level of 0.5 to 0.6 until t=333 ps. This fact indicates that the correlation between $\log_{10}\langle T_{DA}^2\rangle_t$ and $\langle R_{CC}\rangle_t$ remains weak for all the value of t until 333 ps. We have drawn the primary axes for t=2, 20, and 200 ps by the green, blue, and red lines in the Figure 9. We clearly see that

Table 2 Calculated values of the slope $\langle\beta_C\rangle_t$ and ellipticity $\langle\varepsilon\rangle_t$ for some typical average times in the case of center-to-center distance

t	$\langle\beta_C\rangle_t$ (Å^{-1})	$\langle\varepsilon\rangle_t$
1 ps	8.944	0.477
2 ps	9.958	0.469
5 ps	7.058	0.520
10 ps	5.290	0.541
20 ps	4.213	0.477
100 ps	3.812	0.532
200 ps	2.684	0.563
333 ps	2.456	0.615

the slope $\langle\beta_C\rangle_t$ decreases very much with time.

In order to see the time variation of $\langle\varepsilon\rangle_t$ and $\langle\beta_E\rangle_t$ or $\langle\beta_C\rangle_t$ in more detail, we plotted in Figure 10 the diagram for the ellipticity $\langle\varepsilon\rangle_t$ and the slope $\langle\beta_E\rangle_t$ or $\langle\beta_C\rangle_t$ using the data of 90 kinds of t for 1–10 ps, the data points of 18 kinds of t for 10–100 ps and the data points of 8 kinds of t for 100–333 ps. We find that the red line which passes the red circles sharply declines when t is larger than 10 ps and approaches the stationary state value represented by the red square. The evaluation of this point is discussed in the next section. In the case of $\langle\beta_C\rangle_t$, $\langle\varepsilon\rangle_t$ does not decrease until 333 ps.

Using the 10^6 data points for R_{EE} and R_{CC} of 1 ns simulation, we calculate a mean force potential (MFP) as a function of R_{EE} or R_{CC} as follows:

$$F(R_{EE}) = -k_B T \ln\{P(R_{EE})/N\}, \qquad (8)$$

$$F(R_{CC}) = -k_B T \ln\{P(R_{CC})/N\}, \qquad (9)$$

where $P(R_{EE})$ and $P(R_{CC})$ are the frequencies of R_{EE} and R_{CC} which appear in each bin of 0.01 Å, respectively, and N is the total number of the data points. In Figure 11, we plotted the calculated MFP. We found that the simulation points of $F(R_{EE})$ in the upper graph arrange almost in the parabolic form in the region 8.2–10.2 Å. We see that the mean-force potential $F(R_{EE})$ is fitted to the quadratic function very well, although some scatterer is seen in the region 10.2–10.7 Å. The green line is the best fitted curve of the quadratic function of R_{EE}. Similarly, we found that the simulation points of $F(R_{CC})$ of the lower graph arrange almost in the parabolic form in the region 13.2–14.9 Å. We see that the MFP is

fitted to the quadratic function (green line) very well. The curvature of $F(R_{CC})$ is 1.58 time as large as that of $F(R_{EE})$. This fact indicates that the change of the center-to-center distance is harder than that of the edge-to-edge distance.

Discussion

In the first, we evaluate the lower limit of $<\beta_E>_t$ in Figure 10 which corresponds to the value in the stationary state. As we see in Figure 11A, the mean force potential (MFP) as a function of R_{EE} fits very well with the parabolic function in the region 8.5 Å < R_{EE} < 10.0 Å. Therefore, we consider that the fluctuation of the distance in this region is well in the stationary state. We make the histogram for the distribution of R_{EE} using the data of Figure 4. We divide the R_{EE} coordinate into some parts with a bin of 0.02 Å. We count the number of the data points belonging to each bin and select those bins in which the number of the data points involved is larger than 1000. Next we calculate the average value of T_{DA}^2 in each selected bin. In such treatment, the time correlation among $T_{DA}^2(t)$'s and R_{EE} (t)'s is completely neglected. So, we can consider that the average in each bin corresponds to the stationary state. We denote the averaged value of T_{DA}^2 in each bin as $<T_{DA}^2>_S$.

In Figure 12, we plot the value of $\log_{10}<T_{DA}^2>_S$ as a function of R_{EE}. Then, we make the principal coordinate analysis. The obtained primary axis is expressed as

$$\ln<T_{DA}^2>_S = -1.736R_{EE} - 2.421 \qquad (10)$$

Here, the value 1.736 Å^{-1} is the slope $<\beta_E>_S$ in the stationary state. We also evaluate the ellipticity $<\varepsilon>_S$ as 0.058. This data point is plotted in Figure 10 by the red square named S. In Figure 10 we find that the value of $<\varepsilon>_t$ decreases rapidly and ceases to stop at the stationary state as t is increased from 100 ps. The value of $<\beta_E>_t$ decreases slowly from about 2.1 Å^{-1} to the lower limit as t is increased from 100 ps.

Let us consider the mechanism of the property that the values of $<\beta_E>_t$ and $<\beta_C>_t$ are decreased as t is increased and converge to the stationary state value. In the present paper, we have adopted the principal coordinate analysis. In such analysis, the primary axis is chosen along the axis where the dispersion of the data points becomes the largest. When the average time t is small (such as t=2 ps in Figure 8), the dispersion along the $\log_{10}<T_{DA}^2>_t$ axis is much larger than that along the $<R_{EE}>_t$ or the $<R_{CC}>_t$ axis. Then, the slope $<\beta_E>_t$ of the primary axis is large. When t is increased, the dispersion along the $\log_{10}<T_{DA}^2>_t$ axis is decreased considerably but that along the $<R_{EE}>_t$ or the $<R_{CC}>_t$ axis is decreased only slightly. Due to such different behaviors, the slope $<\beta_E>_t$ or $<\beta_C>_t$ of the primary coordinate is decreased when t is increased. The decrease of the slope $<\beta_E>_t$ or $<\beta_C>_t$ ceases when t is very large. The mechanism by which the dispersion along the $\log_{10}<T_{DA}^2>_t$ axis is decreased more rapidly than that along the $<R_{EE}>_t$ or $<R_{CC}>_t$ axis with increase of t is considered as follows: The variation of T_{DA}^2 with time arises

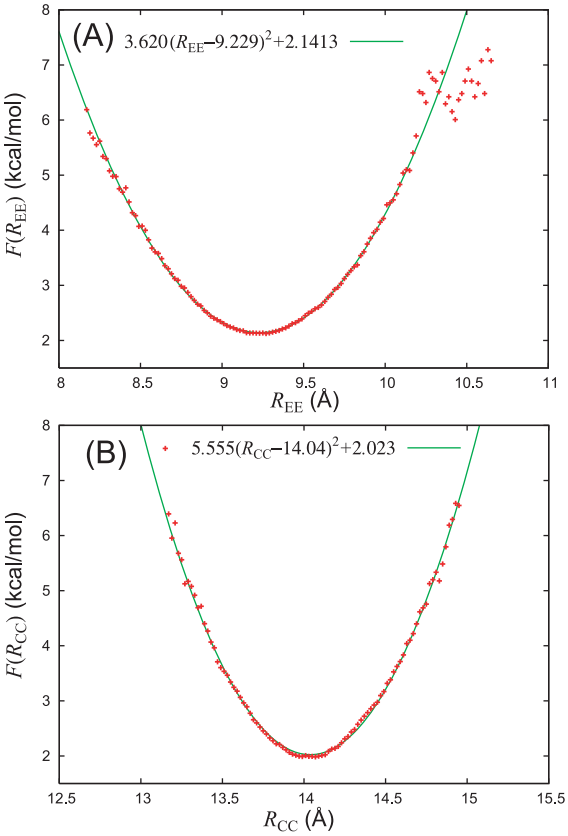

Figure 11 Mean force potentials as a function of R_{EE} (top) and as a function of R_{CC} (bottom). The calculated data points are represented by the red pluses. The fitted parabolic potentials are drawn by green lines.

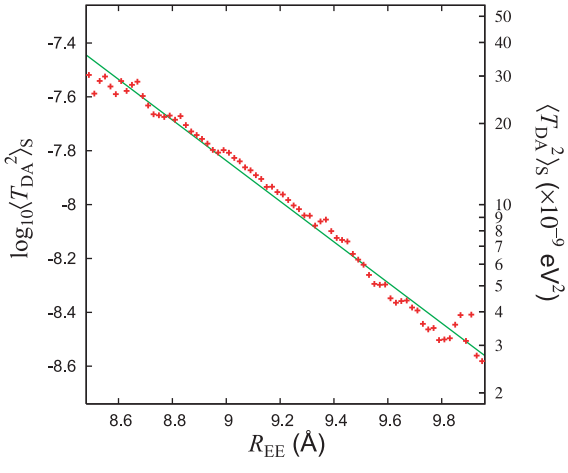

Figure 12 Plot of $\log_{10}<T_{DA}^2>_S$ *vs* R_{EE}. $<T_{DA}^2>_S$ is calculated by averaging T_{DA}^2 which belongs to the bin of R_{EE}. The bin length is 0.02 Å. The green line represents the primary axis.

from the variation of the amino acids conformation as well as the variation of $<R_{EE}>_t$ or $<R_{CC}>_t$. Fast variation of the most amino acids conformation is averaged more rapidly than the slow variation of $<R_{EE}>_t$ or $<R_{CC}>_t$. By such mech-

anism, the dispersion along the $\log_{10}\langle T_{DA}^2\rangle_t$ axis decreases more rapidly than that along the $\langle R_{EE}\rangle_t$ or $\langle R_{CC}\rangle_t$ axis. When t is very large, the fast variation of the amino acids conformation is almost averaged out and the averaged conformation will change in accordance with the variation of $\langle R_{EE}\rangle_t$ or $\langle R_{CC}\rangle_t$. Under such situation, the distribution of $\log_{10}\langle T_{DA}^2\rangle_t$ *vs* $\langle R_{EE}\rangle_t$ or $\langle R_{CC}\rangle_t$ is virtually determined by the variation of $\langle R_{EE}\rangle_t$ or $\langle R_{CC}\rangle_t$. By such mechanism, $\langle\beta_E\rangle_t$ or $\langle\beta_C\rangle_t$ converges to a certain value when t is very large.

In Figure 10 we have also shown that the ellipticity $\langle\varepsilon\rangle_t$ for the edge-to-edge case decreases very much when t is very large, while $\langle\varepsilon\rangle_t$ for the center-to-center case does not decrease from 0.5 when t is very large. This fact will indicate the followings: As we have shown in Figure 2, R_{EE} almost corresponds to the ET route while R_{CC} is not directly correlated with the ET route. Therefore, the correlation between $\log_{10}\langle T_{DA}^2\rangle_t$ and $\langle R_{CC}\rangle_t$ is expected to be a limited one. We can generally say that the correlation between $\log_{10}\langle T_{DA}^2\rangle_t$ and $\langle R_{DA}\rangle_t$ is strong when $\langle\varepsilon\rangle_t$ is small. Therefore, we conclude that the edge-to-edge distance R_{EE} is a better measure of the donor-acceptor distance for the ET than the center-to-center distance. However, we should remind of the fact that the above conclusion will hold true only when the edge-to-edge line is close to the ET route.

So far we have used the average time t as a parameter. This average time has a significant meaning as follows: The probability for the ET is accumulated for each infinitesimal time (1 fs in the present simulation). When the probability is attained to a value of $1/e$ at time t, the ET takes place on the average. Unless the ET rate is very fast, it is reasonable to estimate the value of t by the ET time (inverse of the ET rate in the thermal equilibrium state). The ET time in the present system was experimentally obtained as 200 ps[38]. If we choose t=200 ps, $\langle\beta_E\rangle_t$=1.916 Å^{-1}. Therefore, the β value in the newly found "Dutton law" which holds between the fluctuating distance and fluctuating ET rate in one protein is considerably larger than that of β (1.4 Å^{-1}) corresponding to the ordinary "Dutton law" which holds between the average distance and average ET rate among many redox proteins.

Now, we refer to the analysis of the single-molecule spectroscopy by Yang *et al.* for flavin reductase[17]. The ET time in this system is around 200 ps[17]. Therefore, if the property of the fluctuation of this system is assumed to be similar to ours, the variation of the $\langle T_{DA}^2\rangle_t$ due to variation of R_{EE} in one state remains as represented by the red points in Figure 8. The value of $\langle\beta_E\rangle_t$ at t=200 ps is 1.916 Å^{-1}. Using the data of Figure 8, we evaluated the standard deviation for the fluctuation of $\langle R_{EE}\rangle_t$ as 0.086 Å and for the fluctuation of $\langle T_{DA}^2\rangle_t$ as 1.06 time on the average. These values are relatively small although the used data points (21 points) are much limited. Therefore, we can say that some effect of the rapid fluctuations of R_{EE} and $\langle T_{DA}^2\rangle_t$ in one state (local energy minimum) may be reflected in the average life time γ^{-1} in the single-molecule experiment, but its effect will be small as compared with that of the fluctuation of the possible dynamic disorder due to the transition among many local energy minima.

Using the population of the average life time γ^{-1}, Yang *et al.* calculated the mean force potential (MFP) as a function of the R_{EE} which fluctuates in the time regions of milliseconds to tenseconds[17]. We call the fluctuation in the region of milliseconds to tenseconds the slow fluctuation, hereafter. In such calculation they made use of the ordinary "Dutton law". The calculated MFP is simulated by the parabolic form with curvature 3.2 kcal/mol/Å^2, even though this MFP retains certain skewness. On the other hand, Luo *et al.* calculated the MFP for flavin reductase in the picoseconds region and its curvature was about 8.6 kcal/mol/Å^2 when we read from Figure 2A of Ref. 23. This value is not so much different from the curvature 11.1 kcal/mol/Å^2 of the MFP obtained by the present study in Figure 11B. (It should be reminded that the distance calculated by Luo *et al.* is for the center-to-center distance[23]). From these results we may say that the stochastic property of the distance fluctuation in the picoseconds region is rather similar between the reaction center in our system and the flavin reductase. We call the fluctuations in the region of picoseconds the fast fluctuation, hereafter.

Luo *et al.* also calculated the MFP by applying nine kinds of external potentials to extend the region of the distance fluctuation[23]. By means of the umbrella sampling technique, they calculated the MFP over the wide range of the distance from 6.25 Å to 9.4 Å[23]. It should be noted that this MFP is made of a convolution of the MFP due to the fast fluctuation and the MFP due to the slow fluctuation whose effect was supposed to be incorporated by the umbrella sampling. (Similarly it should be noted that the dispersions of atomic fluctuations in a protein in crystal are made of the dispersions due to the convolution of fast fluctuation and slow fluctuation when one compares the experimentally obtained fluctuation data with the crystallographic data[17]). In order to obtain the MFP due to only the slow fluctuation, it is necessary to deconvolute the MFP due to the fast fluctuation. The deconvolution in the MFP is approximately performed by subtracting the width of the MFP due to the fast fluctuation from the width of the total MFP. This width of the MFP is tentatively measured at the 1 kcal/mol height from the bottom. The calculated result is listed in Table 3. The calculated widths of the MFP of the present system and that of the single-molecule spectroscopy are also listed in the same table. The width (1.0 Å) of the MFP due to the fast fluctuation by Luo *et al.* is similar to the width (0.82 Å) of the MFP of the present system measured by the center-to-center distance although the former is a little larger than the latter. (This result is consistent with the above discussion about the curvature of the MFP). This fact indicates that the property of the fast fluctuation of the present system is rather similar to that of flavin reductase. The width (0.5 Å) of the MFP due to the slow fluctuation of Luo *et al.* measured by the center-to-center distance will be enlarged to 0.64 Å if it

Table 3 Width of the mean force potential at 1 kcal/mol height from the bottom. All the units are in Å

present ET system		flavin reductase			
MD simulation		single-molecule[a]	MD simulation[b]		
edge-to-edge	center-to-center	edge-to-edge	center-to-center		
fast	fast	slow	fast and slow	fast	slow
1.05	0.82	1.7 (0.83)[c]	1.5	1.0	0.5 (0.64)[d]

[a] Yang *et al.*[17] [b] Luo *et al.*[23] [c] Corrected using β=2.0 Å^{-1}. [d] Rescaled by the edge-to-edge distance.

is rescaled by the edge-to-edge distance by the same ratio as Figure 11 in the present system. The width (1.7 Å) of the MFP due to the slow fluctuation obtained by the single-molecule spectroscopy by Yang *et al.* is too large as compared with the above corrected value 0.64 Å. However, if we recalculate the MFP of Yang *et al.* with use of β=2.0 Å^{-1} instead of 1.4 Å^{-1}, the width becomes 0.83 Å, which is close to the above corrected value 0.64 Å of the MD simulation due to only the slow fluctuation. These results indicate that the β value of the "Dutton law" which holds for the slow fluctuation should be also around 2.0 Å^{-1}.

Summarizing the above, we found that the width of the MFP due to the fast fluctuation is similar between the present system and flavin reductase. If one assumes that the β value in the slow fluctuation is 2.0 Å^{-1} or larger, the width of the MFP obtained by the single molecule spectroscopy becomes rather close to the MFP calculated by the MD simulation of umbrella sampling which was supposed to incorporate the slow fluctuation. This fact would indicate that the β value of the "Dutton law" which holds in the fluctuating state is about 2.0 Å^{-1} for the fast and slow fluctuations.

The origin of the above slow fluctuation will be the slow movement of the large portion of the protein. The amplitude of this movement of protein conformation must be of considerably large scale. Accompanied with this slow and large scale of movement of the protein, a slow and small scale of passive movement of the donor-acceptor distance will be induced. At present it is not certain whether the magnitude of the small scale of movement of the donor-acceptor distance is proportional to that of the large scale of movement or not. It is true that only in the case when their movements are directly correlated to each other, the slow and small scale of the movement of donor-acceptor distance can be used as a measure of the slow and large scale of movement of the protein conformation which deserves the name of dynamic disorder. Its check should be made hereafter.

In the above discussion, we have shown that the linear relationship holds true between the fluctuating distance $<R_{EE}>_t$ and the fluctuating $\ln<T_{DA}^2>_t$ for the ET in the RC and also for the ET in flavin reductase. The former ET takes place inside the membrane protein and the latter ET takes place near the surface of the globular protein. Then, we deduce that the above "Dutton law" for the fluctuating state will hold true for many kinds of redox proteins.

Conclusion

In the present study we investigated the correlation between fluctuations of the square of electron tunneling matrix element and the donor-acceptor distance for the ET in the photosynthetic reaction center. At first we found that the distribution in the correlation diagram of $\log_{10} T_{DA}^2$ *vs* R_{EE} or R_{CC} for the instantaneous conformations is very broad. We also found that the dynamic correlation between $\log_{10} T_{DA}^2$ and R_{EE} is very poor even within the correlation time. The distribution of the time-averaged diagram of $\ln<T_{DA}^2>_t$ *vs* $<R_{EE}>_t$ or $<R_{CC}>_t$ was much reduced as the average time t is increased. Applying the principal coordinate analysis, we determined the primary axis from which we obtain the slope $<\beta_E>_t$ or $<\beta_C>_t$. We defined the ellipticity $<\varepsilon>_t$ as the ratio between the standard deviation along the secondary axis and that along the primary axis for each t. The time averaged ellipticity $<\varepsilon>_t$ of the edge-to-edge case remains large value at small value of t until about 10 ps but it becomes rapidly small when t is increased from 10 ps. This fact indicates that the linear relationship between the fluctuation of $\ln<T_{DA}^2>_t$ and the fluctuation of $<R_{EE}>_t$ holds true very well. We found that the value of the slope $<\beta_E>_t$ or $<\beta_C>_t$ decreases very much when t is increased and converges to a certain value in the stationary state. The lower bound of $<\beta_E>_t$ expressed by $<\beta_E>_S$ is 1.74 Å^{-1}, which is larger than the β-value 1.4 Å^{-1} in the ordinary "Dutton law". On the other hand, $<\varepsilon>_t$ of the center-to-center case remains large value even for large values of t. Then, the correlation between $\ln<T_{DA}^2>_t$ and $<R_{CC}>_t$ is worse than that between $\ln<T_{DA}^2>_t$ and $<R_{EE}>_t$. Combining the present results with the MD simulation results of Luo *et al.* and the single-molecule spectroscopic study by Yang *et al.* for flavin reductase, we deduced that the linear relationship between the fluctuation of $\ln<T_{DA}^2>_t$ and the fluctuation of $<R_{EE}>_t$ with larger slope than that of the ordinary "Dutton law" will holds true in many kinds of redox proteins.

Acknowledgement

This work was supported by the Grant-in-Aid on Scientific Research (C) to T.K. from the Ministry of Education, Culture, Sports, Science and Technology of Japan.

References

1. Marcus, R. A. & Sutin, N. Electron transfers in chemistry and biology. *Biochim. Biophys. Acta* **811**, 265–322 (1985).
2. Beratan, D. N., Betts, J. N. & Onuchic, J. N. Protein electron transfer rates set by the bridging secondary and tertiary structure. *Science* **252**, 1285–1288 (1991).
3. Winkler, J. R. Electron tunneling pathways in proteins. *Cur. Op. Chem. Biol.* **4**, 192–198 (2000).
4. Moser, C. C., Keske, J. M., Warncke, K., Farid, R. S. & Dutton, P. L. Nature of biological electron transfer. *Nature* **355**, 796–802 (1992).
5. Page, C. C., Moser, C. C., Chen, X. & Dutton, P. L. Natural engineering principles of electron tunnelling in biological oxidation-reduction. *Nature* **402**, 47–52 (1999).
6. Nishioka, H., Kimura, A., Yamato, T., Kawatsu, T. & Kakitani, T. Interference, fluctuation, and alternation of electron tunneling in protein media. 2. Non-Condon theory for the energy gap dependence of electron transfer rate. *J. Phys. Chem. B* **109**, 15621–15635 (2005).
7. Kakitani, T., Yoshimori, A. & Mataga, N. Theoretical analysis of energy-gap laws of electron-transfer reactions: Distribution effect of donor-acceptor distance. in *Electron Transfer Reaction in Polar Solutions and Electrode Systems, Advances in Chemistry* (Bolton, R., Mataga, N. & McLendon, G. ed.) No. 228, pp. 45–69 (Am. Chem. Soc., 1991).
8. Kakitani, T., Matsuda, N., Yoshimori, A. & Mataga, N. Present and future perspectives of theoretical aspects of the photoinduced charge separation and charge recombination reactions is in solution. *Prog. Reaction Kinetics* **20**, 347–381 (1995).
9. Nishioka, H., Kimura, A., Yamato, T., Kawatsu, T. & Kakitani, T. Interference, fluctuation, and alternation of electron tunneling in protein media. 1. Two tunneling routes in photosynthetic reaction center alternate due to thermal fluctuation of protein conformation. *J. Phys. Chem. B* **109**, 1978–1987 (2005).
10. Vale, R. D., Funatsu, T., Pierce, D. W., Romberg, L., Harada, Y. & Yanagida, T. Direct observation of single kinesin molecules moving along microtubules. *Nature* (London) **380**, 451–453 (1996).
11. Noji, H., Yasuda, R., Yoshida, M. & Kinosita, K. Jr. Direct observation of the rotation of F1-ATPase. *Nature* (London) **386**, 299–302 (1997).
12 Yasuda, R. Noji, H. Kinoshita, K. Jr. & Yoshida, M. F1-ATPase is a highly efficient molecular motor that rotates with discrete 120° step. *Cell* **93**, 1117–1124 (1998).
13. Lu, H. P., Xun, L. & Xie, X. S. Single-molecule enzymatic dynamics. *Science* **282**, 1877–1882 (1998).
14. Zwanzig, R. Rate processes with dynamical disorder. *Acc. Chem. Res.* **23**, 148–152 (1990).
15. Yang, H. & Xie, X. S. Probing single-molecule dynamics photon by photon. *J. Chem. Phys.* **117**, 10965–10979 (2002).
16. Yang, H. & Xie, X. S. Statistical approaches for probing single-molecule dynamics photon-by-photon. *Chem. Phys.* **284**, 423–437 (2002).
17. Yang, H., Luo, G., Karnchanaphanurach, P., Louie, T-M., Rech, I., Cova, S., Xun, L. & Xie, X. S. Protein conformational dynamics probed by single-molecule electron transfer. *Science* **302**, 262–266 (2003).
18. Min, W., Luo, G., Cherayil, B. J., Kou, S. C. & Xie, X. S. Observation of a power-law memory kernel for fluctuations within a single protein molecule. *Phys. Rev. Lett.* **95**, 198302-1–4 (2005).
19. Kou, S. C. & Xie, X. S. Generalized Langevin equation with fractional Gaussian noise: Subdiffusion within a single protein molecule. *Phys. Rev. Lett.* **93**, 180603-1–4 (2004).
20. Granek, R. & Klafter, J. Fractons in proteins: Can they lead to anomalously decaying time autocorrelations? *Phys. Rev. Lett.* **95**, 098106-1–4 (2005).
21. Tang, J. & Marcus, R. A. Chain dynamics and power-law distance fluctuations of single-molecule systems. *Phys. Rev. E* **73**, 022102-1–4 (2006).
22. Wang, J. & Wolynes, P. Passage through fluctuating geometrical bottlenecks. The general Gaussian fluctuating case. *Chem. Phys. Lett.* **212**, 427–433 (1993).
23. Luo, G., Andricioaei, I., Xie, X. S. & Karplus, M. Dynamic distance disorder in proteins is caused by trapping. *J. Phys. Chem. B* **110**, 9363–9367 (2006).
24. Miller, N. E., Wander, M. C. & Cave, R. J. A theoretical study of the electronic coupling element for electron transfer in water. *J. Phys. Chem. A* **103**, 1084–1093 (1999).
25. Castner, E. W. Jr., Kennedy, D. & Cave, R. J. Solvent as electron donor: Donor/Acceptor electronic coupling is a dynamical variable. *J. Phys. Chem. A* **104**, 2869–2885 (2000).
26. Stowell, M. H. B., McPhillips, T. M., Rees, D. C., Soltis, S. M., Abresch, E. & Feher G. Light-induced structural changes in photosynthetic reaction center: Implications for mechanism of electron-proton transfer. *Science* **276**, 812–816 (1997).
27. Morikami, K., Nakai, T., Kidera, A., Saito, M. & Nakamura, H. Presto (Protein engineering simulator): a vectorized molecular mechanics program for biopolymers. *Comput. Chem.* **16**, 243–248 (1992).
28. Cornell, W. D., Cieplak, P., Bayly, C. I., Gould, I. R., Merz, Jr., K. M., Ferguson, D. M., Spellmeyer, D. C., Fox, T., Caldwell, J. W. & Kollman, P. A. A second generation force field for the simulation of proteins, nucleic acids, and organic molecules. *J. Am. Chem. Soc.* **117**, 5179–5197 (1995).
29. Ryckaert, J.-P., Ciccotti, G. & Berendsen, H. J. C. Numerical integration of the Cartesian equations of motion of a system with constraints: molecular dynamics of n-alkanes. *J. Comp. Phys.* **23**, 327–341 (1977).
30. Stewart, J. J. P. Optimization of parameters for semiempirical methods I. Method. *J. Comp. Chem.* **10**, 209-220 (1989).
31. Frisch, M. J., Trucks, G. W., Schlegel, H. B., Scuseria, G. E., Robb, M. A., Cheeseman, J. R., Zakrzewski, V. G., Montgomery, Jr., J. A., Stratmann, R. E., Burant, J. C., Dapprich, S., Millam, J. M., Daniels, A. D., Kudin, K. N., Strain, M. C., Farkas, O., Tomasi, J., Barone, V., Cossi, M., Cammi, R., Mennucci, B., Pomelli, C., Adamo, C., Clifford, S., Ochterski, J., Petersson, G. A., Ayala, P. Y., Cui, Q., Morokuma, K., Malick, D. K., Rabuck, A. D., Raghavachari, K., Foresman, J. B., Cioslowski, J., Ortiz, J. V., Baboul, A. G., Stefanov, B. B., Liu, G., Liashenko, A., Piskorz, P., Komaromi, I., Gomperts, R., Martin, R. L., Fox, D. J., Keith, T., Al-Laham, M. A., Peng, C. Y., Nanayakkara, A., Challacombe, M., Gill, P. M. W., Johnson, B., Chen, W., Wong, M. W., Andres, J. L., Gonzalez, C., Head-Gordon, M., Replogle, E. S. & Pople, J. A. *Gaussian98*, revisionA.9 (Gaussian, Inc., Pittsburgh PA, 1998).
32. Howell, J., Rossi, A., Wallace, D., Haraki, K. & Hoffmann, R. *FORTICON8* (Extended Hückel program.) (Quantum chemistry program exchange, Indiana Univ., Bloomington, IN), *QCPE* **11**, No. 344 (1977).
33. Nishioka, H. & Kakitani, T. Average electron tunneling route of the electron transfer in protein media. *J. Phys. Chem. B* **112**, 9948–9958 (2008).
34. Kawatsu, T., Kakitani, T. & Yamato, T. Destructive interference in the electron tunneling through protein media. *J. Phys. Chem. B* **106**, 11356–11366 (2002).
35. Tan, M.-L., Balabin, I. A. & Onuchic, J. N. Dynamics of electron transfer pathways in Cytochrome *c* Oxidase. *Biophys. J.* **86**, 1813–1819 (2004).
36. Lin, J., Balabin, I. A. & Beratan, D. N. The nature of aqueous tunneling pathways between electron-transfer proteins. *Science* **310**, 1311–1313 (2005).
37. Prytkova, T. R., Kurnikov I. V. & Beratan, D. N. Coupling coherence distinguishes structure sensitivity in protein electron transfer. *Science* **315**, 622–625 (2007).
38. Gunner, M. R. & Dutton, P. L. Temperature and $-\Delta G°$ dependence of the electron transfer from BPh^- to Q_A in reaction center protein from *Rhodobacter sphaeroides* with different quinones as Q_A. *J. Am. Chem. Soc.* **111**, 3400–3412 (1989).